Original Article

Sprouty1 Prevents Cellular Senescence Maintaining Proliferation and Differentiation Capacity of Human Adipose Stem/Progenitor Cells

Markus Mandl, PhD,[1,2,†] Sonja A. Wagner, MSc,[1,2,†] Florian M. Hatzmann, MSc,[1,2] Asim Ejaz, PhD,[1,3] Heike Ritthammer, MSc,[1] Saphira Baumgarten, MSc,[1] Hans P. Viertler, MSc,[1,2] Jochen Springer, BSc,[1] Marit E. Zwierzina, MD,[4] Monika Mattesich, MD,[4] Camille Brucker, MSc,[1] Petra Waldegger, BSc,[1,2] Gerhard Pierer, MD,[4] and Werner Zwerschke, PhD[1,2,*]

[1]Division of Cell Metabolism and Differentiation Research, Research Institute for Biomedical Aging Research, University of Innsbruck, Austria. [2]Center for Molecular Biosciences Innsbruck (CMBI), University of Innsbruck, Austria. [3]Present address: Adipose Stem Cell Center, Department of Plastic Surgery, University of Pittsburgh, Pennsylvania. [4]Department of Plastic and Reconstructive Surgery, Innsbruck Medical University, Austria.

[†]These authors contributed equally to this work.

*Address correspondence to: Werner Zwerschke, PhD, Division of Cell Metabolism and Differentiation Research, Research Institute for Biomedical Aging Research, University of Innsbruck, Rennweg 10, 6020 Innsbruck, Austria. E-mail: werner.zwerschke@uibk.ac.at

Abstract

The role of Ras-Mitogen-activated protein kinase (MAPK) signaling in cellular aging is not precisely understood. Recently, we identified Sprouty1 (*SPRY1*) as a weight-loss target gene in human adipose stem/progenitor cells (ASCs) and showed that Sprouty1 is important for proper regulation of adipogenesis. In the present study, we show that loss-of-function of Sprouty1 by CRISPR/Cas9-mediated genome editing in human ASCs leads to hyper-activation of MAPK signaling and a senescence phenotype. Sprouty1 knockout ASCs undergo an irreversible cell cycle arrest, become enlarged and stain positive for senescence-associated β-galactosidase. Sprouty1 down-regulation leads to DNA double strand breaks, a considerably increased number of senescence-associated heterochromatin foci and induction of p53 and p21^{Cip1}. In addition, we detect an increase of hypo-phosphorylated Retinoblastoma (Rb) protein in *SPRY1* knockout ASCs. p16^{Ink4A} is not induced. Moreover, we show that Sprouty1 knockout leads to induction of a senescence-associated secretory phenotype as indicated by the activation of the transcription factors NFκB and C/EBPβ and a significant increase in mRNA expression and secretion of interleukin-8 (IL-8) and CXCL1/GROα. Finally, we demonstrate that adipogenesis is abrogated in senescent *SPRY1* knockout ASCs. In conclusion, this study reveals a novel mechanism showing the importance of Sprouty1 for the prevention of senescence and the maintenance of the proliferation and differentiation capacity of human ASCs.

Keywords: Adipogenesis, Adipose stem cell, Obesity, Senescence, Sprouty1

Obesity is a world-wide public health issue (1) that increases the risk of illness and shortens life span (2,3). This metabolic disorder is characterized by an excessive increase in white fat mass resulting in dysfunctional adipose tissue. The gain of adipose tissue mass is achieved due to an increased size of adipocytes (hypertrophy) and to proliferation and differentiation of adipose stem/progenitor cells (ASCs) generating new adipocytes (hyperplasia) (4,5). While the detrimental effects of obesity are not completely understood, increasing evidence suggests that it may accelerate the aging process (6–8). Obesity is linked to cellular aging (7) and age-related diseases (6–8). Moreover, it has been shown that adipose tissue dysfunctions correlate with aging and are associated

with increasing numbers of senescent ASCs and aged adipocytes (7,9–13).

According to the current model, cellular senescence is defined as a permanent cell cycle arrest that is induced when cells are exposed to various stress signals (premature senescence) or are reaching the end of their replicative life span (replicative senescence) (14). This cell state plays an important role in organismal aging, tumor suppression, tissue homeostasis, and development (14–16). Cellular senescence is a multistep process established by the activation of the p16[Ink4a] and/or the p53/p21[Cip1] pathways and the Retinoblastoma (Rb) family proteins, whereas other mechanisms might exist. Senescent cells are characterized by features such as a flat morphology in culture, senescence-associated β-Galactosidase (SA β-Gal) positivity, the appearance of senescence-associated heterochromatic foci (SAHF), and the secretion of a distinct pattern of factors, known as the senescence-associated secretory phenotype (SASP) (14,17). Depending on the exact composition, SASP factors can exert deleterious effects in an autocrine, paracrine, and systemic manner and contribute to the aging process (17).

Interventions to treat obesity reduce fat mass, promote longevity in animal models (18,19) and elicit health benefits in humans (2,3,20,21). Mechanisms on how weight-loss (WL) interventions improve health span are a current focus of obesity and aging research. Especially their impact on ASCs is little understood. We have shown that WL reduces the adipogenic activity, protects against DNA-damage, and extends the replicative life span of human ASCs (22) and identified WL-target genes in these cells (9,23,24). One of these genes, which is upregulated in ASCs of formerly obese people, is *SPRY1* encoding for Sprouty1, a negative regulator of the Ras-Mitogen-activated protein kinase (MAPK) pathway (23,25). The activity of this pathway is triggered by binding of mitogens or growth factors to appropriate receptor tyrosine kinases (RTKs) followed by receptor autophosphorylation and recruitment of adaptor proteins that facilitate phosphorylation events leading to activation of the MAPK extracellular signal-regulated kinase 1/2 (ERK1/2) (26,27). Nuclear translocation of phosphorylated ERK enables the activation of certain transcription factors and induction of genes required for cell proliferation, differentiation and other processes (26,27). The transient nature of the signal relayed is maintained by negative feedback-loops (26). The induction of the repressors of the Sprouty family allows a time delay and modulation of ERK1/2 dynamics (26). They are expressed in response to MAPK signaling and intercept this pathway at various nodes (28). Sprouty1 (*SPRY1*) has been demonstrated to play a role in adipose tissue (29). Moreover, it was demonstrated that Sprouty1 is important for switching between proliferation and quiescence in muscle stem cells in order to maintain the self-renewal capacity of this cell type throughout life (30–33).

We recently showed that Sprouty1 is necessary for proper regulation of adipogenic differentiation in ASCs (23). Since WL postpones replicative senescence in human ASCs (22) and the MAPK-pathway plays an important role in the regulation of cell proliferation and senescence (34,35), the objective of this study was to analyze whether Sprouty1 is linked to cellular senescence in human ASCs. By employing a CRISPR/Cas9-mediated loss-of-function approach, we demonstrate that Sprouty1 depletion leads to augmented MAPK activation, cessation of cell cycle progression, the induction of a cellular senescence phenotype, and inhibition of adipogenesis.

Materials and Methods

Ethics Declaration and Donor Characteristics

Subcutaneous white adipose tissue (sWAT) samples were obtained from patients undergoing routine elective plastic abdominal surgery at the Institute for Plastic and Reconstructive Surgery (Medical University of Innsbruck, Austria). All patients gave their informed written consent. The study protocol was approved by the Ethics Committee of the Medical University of Innsbruck (Austria) according to the Declaration of Helsinki. For this study, sWAT samples of n = 13 healthy donors of Caucasian origin were used (Supplementary Table 1).

Isolation of Human Adipogenic Stromal/Progenitor Cells (ASCs) and Cell Culture

ASC isolation and cultivation was done as described in our previous study (23).

Cloning Procedures

CRISPR/Cas9-encoding vectors targeting *SPRY1* were generated in accordance with the Genome-Scale CRISPR Knock-Out (GeCKO) protocol (36,37). Sequences of DNA oligos required for cloning into the linearized lentiCRISPR.v2 vector (Addgene plasmid # 52961; http://n2t.net/addgene:52961; described in Ref. (36)) are given in Supplementary Table 2. As a negative control, a CRISPR/Cas9 target sequence against the Green Fluorescent Protein (GFP), which has no effects on the human genome (38,39), was cloned into the lentiCRISPR.v2 vector (Supplementary Table 2). All plasmids were amplified in *Escherichia coli* Stbl3 bacteria. Endotoxin-free plasmid preparations for transfection were gained using the EndoFree Plasmid MaxiKit (Qiagen) or the GeneJET Endo-free Plasmid Maxiprep Kit (Thermo Scientific) according to the manufacturer's protocol. For RNA interference-mediated gene silencing, a set of five pLKO.1 plasmids encoding different shRNAs targeting the human *SPRY1* gene were purchased from a commercial supplier (Dharmacon, TRCN00000 5693-3 to -7; in this study: TRCN00000 5693–5 is referred to as shRNA#1, -6 is referred to as shRNA#2) and tested previously (23). For comparison, an appropriate nontargeting control was used (24).

Generation of Lentiviral Particles

Lentiviral particles for gene transduction were produced and titrated as previously described (24,40). Lentiviruses were stored at –80°C until use.

Infection of ASCs

ASCs were infected with the given lentiCRISPRv2 viruses and selected by antibiotic resistance as previously described (23). Lentivirus-transduced ASCs were Puromycin-selected (2 µg/mL) for at least 3 days. Subsequently, the entire cell population was used for the analysis. Transduction efficiency of lentiviruses expressing the CRISPR/Cas9 knock out system was routinely confirmed by transducing a U2OS cell line stably expressing GFP – LC3 with the lentiCRISPRv2 expressing gRNACtr targeting green fluorescent protein (GFP). After cell transduction followed by Puromycin selection, gRNA targeting GFP abolished GFP fluorescence in > 90% of the U2OS – GFP – LC3 cells.

Differentiation of ASCs

ASCs were seeded in six-well plates at a density of 2×10^4 cells/cm^2 followed by adipogenic differentiation as described in Ref. (9).

Quantification of Intracellular Lipids

Intracellular lipids were stained with Oil Red O (ORO) as described in Ref. (9). For quantification, ORO was redissolved with 1 mL Isopropanol for 30 minutes and absorbance was measured at 570 nm.

Western Blot Analysis

Western blotting was performed as described previously (23). Primary antibodies are listed in Supplementary Table 3. To ensure equal loading of samples, PVDF membranes were incubated with a β-Actin antibody (1:100,000; Sigma–Aldrich, AC-15, #A5441) for 1 hour at room temperature. Appropriate secondary HRP-conjugated antibodies (Anti-Mouse IgG, #W402B, Promega; Polyclonal Swine Anti-Rabbit IgG, #P0399, DAKO) were diluted 1:5,000 and applied for 1 hour at room temperature. Densitometric quantification of X-ray films was performed using ImageJ software (version 1.47, National Institutes of Health, USA).

Immunocytochemistry

ASCs were seeded on sterile cover slips (diameter 15 mm) placed in six-well plates at a density of 2,600 cells/cm^2 in ASC2 medium. Next day, the supernatant was replaced by PM4 growth medium and the cells were cultured for 3 days. Subsequently, cells were washed twice with ice-cold PBS and fixed with 4% w/v Paraformaldehyde/ PBS for 20 minutes at room temperature. Permeabilization of cells was achieved by treatment with Permeabilization buffer (0.5% Triton-X100 and 0.1% Sodium citrate in PBS) for 5 minutes on ice followed by blocking of unspecific binding sites with 1%BSA/ PBS for 10 minutes. Antibodies (anti- γ -H2A.X, Abcam, #ab18311; anti-Ki67, Thermo Scientific, #RM-9106-S0; anti-p65, Santa Cruz Biotechnology, #sc-372) were diluted 1:100 and applied overnight. Cover slips were washed three times with 1%BSA/PBS and incubated with the secondary antibody (Goat Anti-Rabbit IgG Alexa Fluor 488, Invitrogen) diluted 1:300 for 1 hour at room temperature. An appropriate control staining without primary antibody was used as negative control to confirm specificity of the signal. 4′,6-Diamidin-2-phenylindol (DAPI) was used for counter-staining to visualize cell nuclei. Finally, cover slips were washed twice in 1%BSA/PBS and PBS, respectively, and mounted. Images were taken using a CellVoyager CV1000 Imaging System (Visitron Systems).

5-Bromo-2′-deoxy-uridine (BrdU) Incorporation Assay

To determine ASC proliferation, cells were seeded in 96-well plates (ASC medium supplemented with 10% fetal calf serum [FCS]) at a density of 5.3 × 10^3 cells/cm^2 and allowed to attach overnight. BrdU labeling was performed in PM4 medium using the 5-Bromo-2′-deoxy-uridine Labeling and Detection Kit III (Roche) in accordance with the manufacturer's protocol. Optical density was measured after 4 days of incubation using a plate reader (Infinite M200, TECAN).

Growth Curves

ASCs were seeded in six-well plates at a density of 5 × 103 cells/cm^2 (ASC medium supplemented with 10% FCS) and allowed to attach overnight. Next day, the supernatant was replaced by fresh PM4 medium. This time point was referred to as day 0. For counting, three wells were harvested by trypsinization at each time point. Viable cells of each well were counted twice using a Neubauer chamber in conjunction with Trypan blue exclusion.

Senescence-Associated (SA) β-Galactosidase (β-Gal.) Staining

ASCs were seed in six-well plates at a density of 5 × 103 cells/ cm^2 (ASC medium supplemented with 10% FCS) and incubated overnight. On the next day, the supernatant was discarded and replaced by PM4 medium. ASCs were cultured for one additional day and subjected to SA β-Gal. staining as described previously (9). Subsequently, microphotographs were taken and cells were counted using ImageJ software (version 1.47, National Institutes of Health).

Mutation Detection Assay

To determine the extent of CRISPR/Cas9-mediated mutation of the *SPRY1* gene, the Guide-it Mutation Detection Kit (Takara Bio USA, Inc.) was used according to the manufacturer's guidelines. The appropriate genomic locus was amplified by a three-step PCR with the following primer pair (CRISPR/SPRY1_Detection_f: ATCAAGGCCATAAGAGGCAGC; CRISPR/SPRY1_Detection_r: AGTTAGACCTTGGCAACAGGG) as described by the manufacturer's instructions. PCR- and cleavage products were dissolved onto a 2% Agarose/TAE gel containing Midori Green and visualized by a transiluminator.

Gene Expression Analysis

Gene expression was analyzed as described previously (24). The RNeasy Plus Micro Kit (Qiagen, #74034) was used to isolate total RNA in accordance with the manufacturer's protocol. cDNA synthesis was performed using the First Strand cDNA Synthesis Kit (Thermo Scientific, #K1622) as described in the supplier's guidelines. Primer sequences for quantitative real-time polymerase chain reaction (qPCR) are given in Supplementary Table 4. Gene expression was measured with a LightCycler 480 (Roche) instrument using SYBR green chemistry.

Cytokine Array

Transduced and Puromycin-selected ASCs were seeded in six-well plates at a density of 5 × 103 cells/cm^2 and incubated overnight. On the next day, the supernatant was aspirated and replaced by 1 mL/well PM4 medium for 72 hours. Conditioned media were collected and cells were harvested to gain RNA and protein samples, respectively. Culture supernatants were stored immediately at −80°C until analysis. Corresponding supernatants of three different donors were equally mixed and analyzed by the Proteome Profiler Human Cytokine Array (RnDSystems, #ARY005B) as described in the manufacturer's instructions. This array can detect 36 different cytokines. Development of the signal was achieved with the Western Lightning Plus ECL reagent (PerkinElmer) and membranes were exposed to a medical X-ray film (Super RX-N, FUJI) for up to 60 minutes. Quantification was performed with ImageJ software (version 1.47, National Institutes of Health).

Enzyme-Linked Immunosorbent Assay (ELISA)

Appropriate cytokines secreted in the cell culture supernatant were measured using the following ELISA kits according to the manufacturer's protocol: CXCL1: Human GRO-α/MGSA (CXCL1) ELISA development kit (Peprotech, #900-M38); IL-6: Human IL-6 ELISA MAX Deluxe (BioLegend, #430905); IL-8: Human IL-8 ELISA (Invitrogen by ThermoScientific, #88-8086-88).

Statistics

Statistical analysis was performed with GraphPad Prism 5 software (GraphPad Software Inc., La Jolla, CA). Each experiment was conducted with a minimum of $n = 3$ biological replicates (ie, donors). All measurements were done in triplicates. All values are given as mean ± SEM. Statistical comparison was achieved using the unpaired two-tailed *t*-test or analysis of variance depending on the type of the data set and as indicated in the corresponding figure legend. *p* values ≤ .05 were considered to be significant.

Results

CRISPR/Cas9-Mediated SPRY1 Knockout Augments MAPK Signaling and Induces Premature Senescence in Human ASCs

Recently, we demonstrated that Sprouty1 is crucial for ASCs to maintain the adipogenic differentiation capacity (23). However, the underlying mechanism is not precisely understood. Since Sprouty1 negatively regulates Ras-MAPK signaling and hyper-activation of this mitogenic pathway is associated with oncogene-induced senescence (15), we hypothesize that Sprouty1 is necessary for maintaining the balance between proliferation, senescence, and differentiation in ASCs. To address this issue, we generated a *SPRY1* loss-of-function phenotype using a CRISPR/Cas9 all-in-one system and the guide RNA (gRNA) CRISPR-construct #1 to target the *SPRY1* gene in primary human ASCs. The CRISPR/Cas9 target sequence against Green Fluorescent Protein (GFP) served as a negative control. The disruption/knockout (KO) of the human *SPRY1* gene was confirmed using a mutation detection assay (Figure 1A). Moreover, Western blot analysis revealed an inhibited Sprouty1 protein expression in CRISPR/Cas9-mutated ASCs compared to control cells (Figure 1B).

To investigate whether *SPRY1* KO ASCs are hyper-responsive to MAPK signaling, cells were serum-starved, stimulated with PM4 growth medium, and analyzed by Western blotting. As expected, an augmented ratio of phosphorylated ERK1/2 was detected in *SPRY1* KO ASCs compared to the control (Figure 1C). Next, we determined the effect of *SPRY1* KO on cell proliferation by establishing growth curves and performing BrdU incorporation assays. As presented in Figure 1D and E, *SPRY1* KO ASCs showed a proliferation arrest, CRISPR-GFP expressing cells served as negative control. Moreover, the antiproliferative effect observed in *SPRY1* KO ASCs was associated with significantly increased numbers of senescence-associated (SA) β-Galactosidase (β-Gal) positive ASCs (Figure 1F and G) and decreased Ki67 abundancy (Figure 1H and I). Apoptosis was not observed in CRISPR/Cas9 transduced ASCs as determined by Annexin V/PI staining (Supplementary Figure S1). Taken together, these results demonstrate the importance of Sprouty1 to maintain the proliferative capacity of human ASCs and to prevent cellular senescence due to augmented RAS-MAPK signaling.

Knockdown of Sprouty1 by RNA Interference Phenocopies SPRY1 KO and Triggers Cellular Senescence in Human ASCs

To confirm the effects observed in *SPRY1* KO ASCs, a gene-silencing approach using RNA interference was employed. Therefore, ASCs were transduced with lentiviruses encoding two different shRNAs (shRNA #1 and #2) targeting the Sprouty1 mRNA or a nontargeting

control. As shown in Figure 2A, Sprouty1 protein was depleted by both shRNA #1 and shRNA #2 and silencing of Sprouty1 elevated the abundance of phosphorylated ERK1/2 in PM4-stimulated ASCs compared to shCtrl indicating augmented MAPK activation (Figure 2B). Growth curves revealed an antiproliferative effect of Sprouty1 knockdown (KD) in ASCs (Figure 2C), which was further confirmed by a significantly reduced BrdU incorporation compared to control cells (Figure 2D). In addition, the antiproliferative phenotype of Sprouty1 KD ASCs was accompanied by a flat cellular morphology and increased SA β-Gal positivity (Figure 2E). In conclusion, shRNA-mediated knockdown of Sprouty1 induced an antiproliferative and senescent phenotype similarly as observed in *SPRY1* KO ASCs and confirms the key role of Sprouty1 in balancing ASC proliferation and senescence.

SPRY1 KO Induces a Distinct Senescence Phenotype in Human ASCs

We further elucidated the molecular mechanism underlying *SPRY1* KO-mediated senescence. *SPRY1* KO ASCs showed a considerable upregulation of p53 (Figure 3A) and its target p21^{Cip1} (Figure 3B) associated with Rb activation (hypo-phosphorylation; Figure 3C). In addition, immunostaining of the histone modification γ-H2A.X revealed the appearance of DNA double-strand breaks which were associated with senescence-associated heterochromatin foci (SAHF) in *SPRY1* KO cells (Figure 3D and E). These results confirm the senescent phenotype in *SPRY1* KO ASCs and reveal a p53/p21^{Cip1}-dependent mechanism.

Next, we analyzed whether the knockout of Sprouty1 induced a senescence-associated secretory phenotype (SASP) in the ASCs. To do this, we analyzed the supernatants of CRISPR-construct #1 and CRISPR-GFP ASCs by a cytokine array (Supplementary Figure S2). While both CRISPR-GFP transduced and SPRY1 KO ASCs secreted CCL2/MCP-1, CXCL12/SDF-1, interleukin (IL)-6, MIF, and Serpin E1/PAI-1 at a detectable concentration (Figure 4A), the *SPRY1* KO ASCs additionally released CCL1/I-309, CXCL1/GROα, and IL-8 (Figure 4A). To confirm the results obtained from the cytokine array, we performed ELISA measurements of corresponding cell culture supernatants. CCL1 was not detectable by ELISAs but as shown in Figure 4B, IL-8 and CXCL1/GROα, both are signature cytokines of senescent cells (14,17), were significantly elevated in *SPRY1* KO ASCs compared to control cells. These effects were also mirrored on mRNA level (Figure 4C). Since IL-6 is a frequent component of SASPs and its levels were relatively high in both CRISPR-construct #1 and CRISPR-GFP ASCs, IL-6 was also examined by qRT-PCR analysis and ELISA. While we detected significantly increased IL-6 mRNA levels in Sprouty1 KO ASCs derived from three different donors, the IL-6 levels in the given supernatants were not significantly increased. Taken together, we identified a unique SASP pattern in *SPRY1* KO ASCs which includes IL-8 and CXCL1/GROα. Mechanistically, it has been shown that the transcription factors C/EBPβ and NF-κB activate the expression of genes coding for proteins belonging to the SASP (17). Therefore, we tested whether C/EBPβ and NF-κB are activated in response to *SPRY1* KO. As shown in Figure 4D C/EBPβ protein was significantly elevated in *SPRY1* KO ASCs and nuclear translocation of the NF-κB subunit p65 was significantly increased in these cells indicating an active NF-κB pathway (Figure 4E). These findings underscore that the knockout of *SPRY1* in human ASCs specifically induces an SASP.
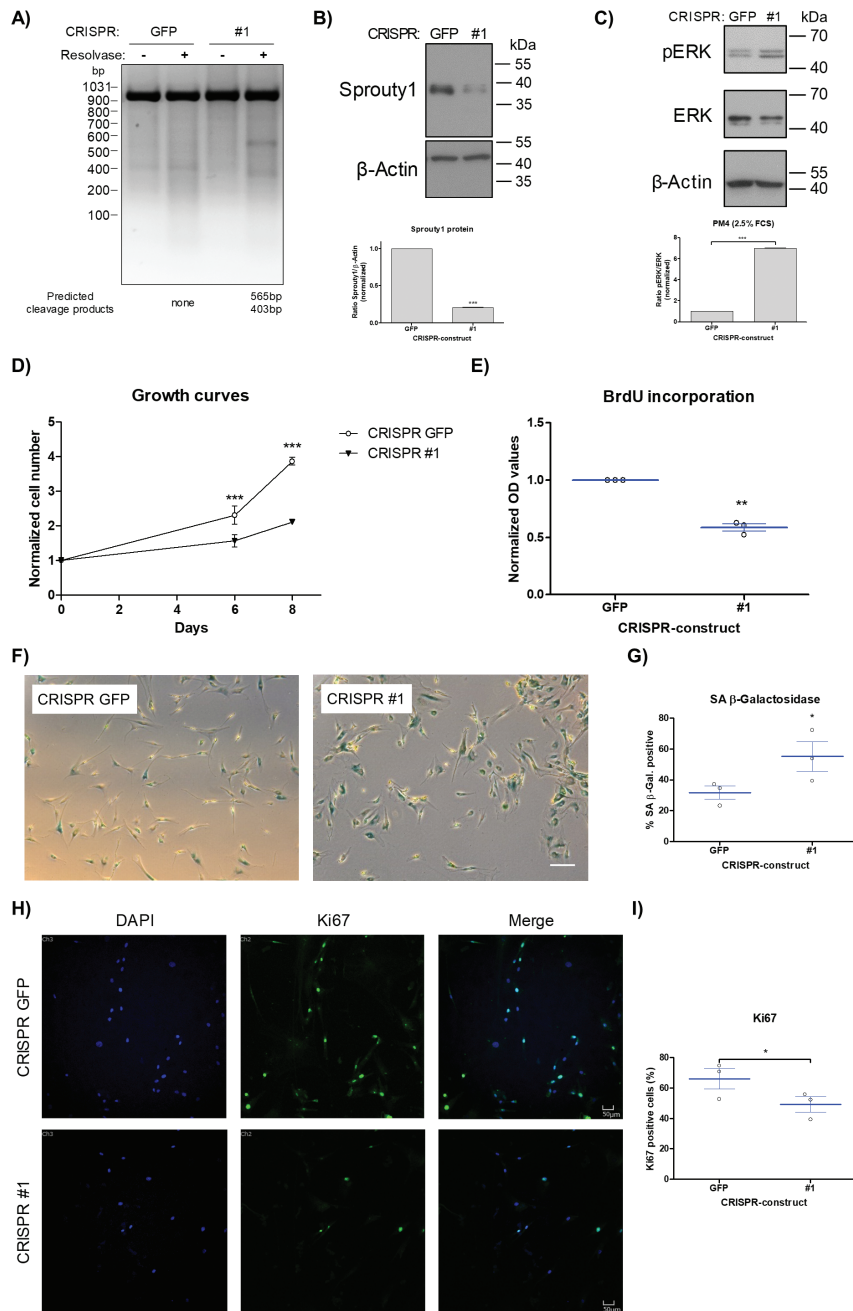
Figure 1. CRISPR/Cas9-mediated knockout of *SPRY1* in human adipose stem/progenitor cells (ASCs) and its effects on proliferation. (**A**) Mutation-detection assay of ASCs transduced either with CRISPR-construct #1 targeting an appropriate sequence within the *SPRY1* gene or with CRISPR GFP targeting the Green Fluorescent Protein gene (GFP; negative control). The intended CRISPR/Cas9 genomic target region within the *SPRY1* locus was polymerase chain reaction (PCR) amplified and the PCR product rehybridized, followed by Resolvase treatment to cleave mutated/mismatched DNA strands. Subsequently, cleavage products were visualized on a 2% agarose gel. Fragment sizes are indicated in bp. No specific Resolvase-mediated cleavage of the PCR product was observed in CRISPR-GFP control cells, whereas fragments of predicted length were detected in CRISPR-construct #1 transduced ASCs. A representative result of $n = 3$ different donors is shown. (**B**) Western blot analysis of CRISPR/Cas9 transduced ASCs expressing CRISPR-construct #1 and CRISPR-GFP. Upper panel: A representative Western blot result in ASCs of $n = 3$ independent donors is shown. β-Actin served as loading control. Molecular masses are given in kDa. Lower panel: Densitometry of the Western blot shown. Values are presented as mean ± SEM of three measurements. Statistical comparison was performed using the paired two-tailed *t*-test. (**C**) Proliferating CRISPR/Cas9 expressing ASCs were serum-starved for 2 days followed by short-term stimulation (15 minutes) with PM4 medium and Western blot analysis of MAPK signaling. Upper panel: Representative Western blot result of $n = 3$ independent experiments (ie, donors). β-Actin served as loading control. Molecular masses are given in kDa. Lower panel: Densitometric quantification of the Western blot shown. Values are presented as mean ± SEM of three measurements. Statistical comparison was done using the paired two-tailed *t*-test. (**D**) Growth curves of CRISPR/Cas9-transduced ASCs. Cell counting was performed using a Neubauer chamber. Representative result of $n = 3$ independent experiments (ie, donors). Statistical comparison was achieved using two-way ANOVA and Bonferroni post hoc test. (**E**) Measurement of ASC proliferation by BrdU incorporation in ASCs from $n = 3$ different donors. OD values were normalized to corresponding CRISPR-GFP control cells. Statistical analysis among donors was performed using the paired two-tailed *t*-test. (**F**) Senescence-associated (SA) β-Galactosidase (β-Gal) staining of CRISPR/Cas9-expressing and control (GFP) ASCs. Representative images of ASCs from $n = 3$ different donors are shown. Magnification 50×. Scale bar: 200 μm. (**G**) Quantification of SA β-Gal-positive ASCs performed with cells from $n = 3$ different donors. Statistical analysis among donors was conducted using the one-tailed paired *t*-test. (**H**) Expression of the proliferation marker Ki67 in CRISPR/Cas9-transduced ASCs. Representative microphotographs of immunocytochemically stained ASCs from one out of three different donors are shown. Scale bar: 50 μm. (**I**) Quantitation of Ki67-positive cells among $n = 3$ different donors. At least 500 cells were counted per condition/donor. Values are presented as mean ± SEM. Statistical comparison was done using the Two-tailed Paired *t*-test. Full color version is available within the online issue.
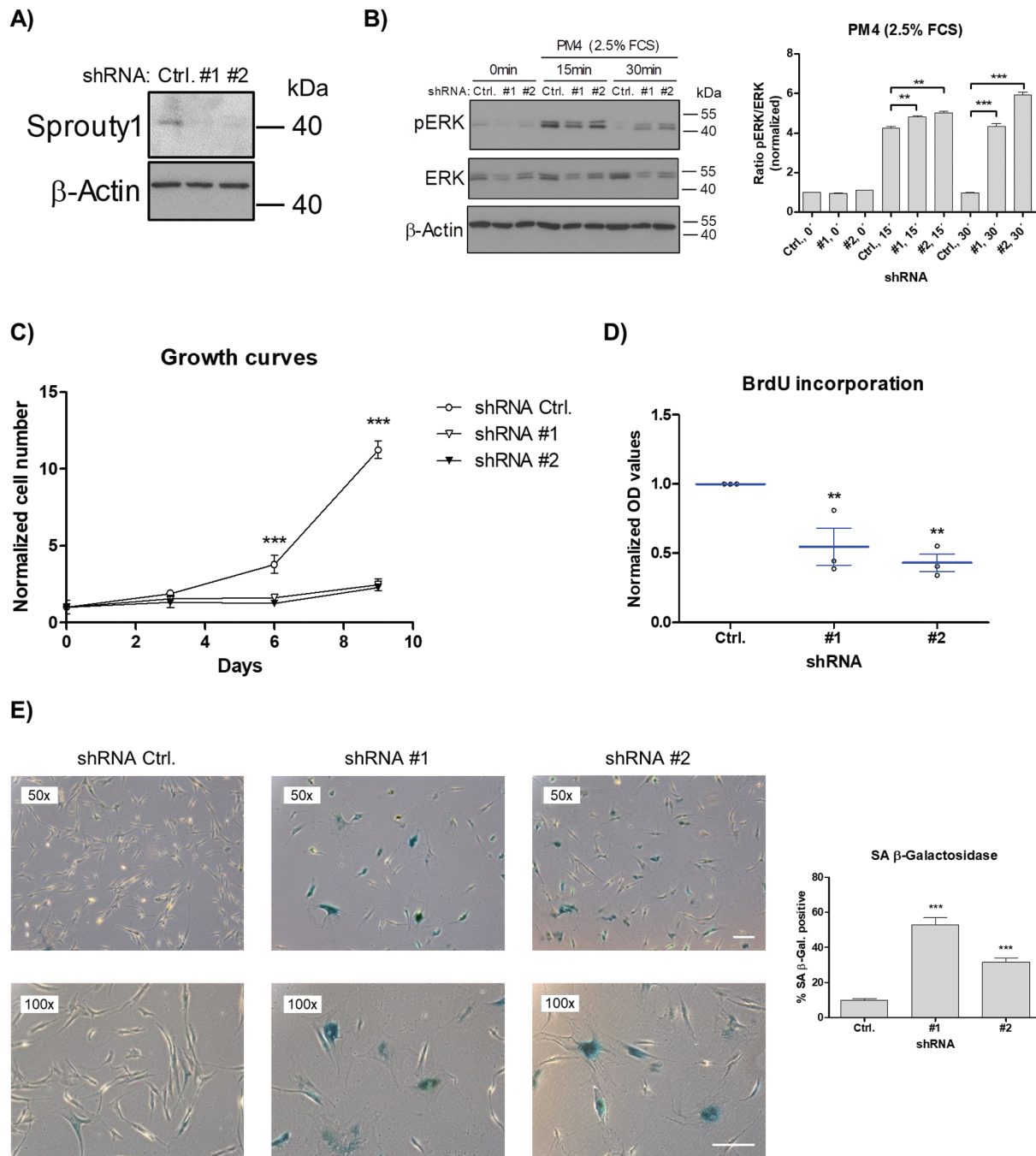
Figure 2. Effects of Sprouty1 knockdown (KD) in proliferating ASCs. (**A**) Western blot analysis of shRNA-transduced adipose stem/progenitor cells adipose stem/ progenitor cells (ASCs). A nontargeting control shRNA (shCtrl) and two distinct shRNAs targeting Sprouty1 (*SPRY1*) mRNA (shRNA#1, shRNA#2) were used. A representative Western blot result using anti Sprouty1 antibodies from ASCs of *n* = 3 independent donors is shown. β-Actin was assayed as loading control. Molecular masses are given in kDa. (**B**) shRNA-transduced ASCs were serum-starved for 2 days followed by short-term stimulation with PM4 growth medium for defined time points as indicated and analyzed by Western blotting using antibodies against pERK and ERK. Left panel: A representative result of *n* = 3 independent experiments (ie, donors) is shown. β-Actin served as loading control. Molecular masses are given in kDa. Right panel: Densitometric quantification corresponding to the Western blot shown. Statistical comparison was achieved using the Unpaired two-tailed *t*-test. Values are presented as mean ± SEM of three measurements. (**C**) Growth curves of Sprouty KD ASCs. Cells were counted at indicated time points using a Neubauer chamber. Representative result of *n* = 3 different experiments (ie, donors). Statistical comparison was achieved using two-way ANOVA and Bonferroni post hoc test. (**D**) DNA synthesis determined by BrdU incorporation is shown. Data from ASCs of *n* = 3 different donors measured in triplicates are shown. Values are presented as mean ± SEM. Statistical comparison was done using one-way ANOVA with Dunnett's Multiple Comparison test. (**E**) Senescence-associated (SA) β-Galactosidase (β-Gal) staining of Sprouty1 KD and control ASCs. Left panel: Representative images of ASCs from *n* = 3 different donors are shown. Magnification 50× and 100× as indicated. Scale bar: 200 µm. Right panel: Quantification of SA β-Gal-positive cells corresponding to the microphotographs shown. Statistical comparison was achieved using the two-tailed Unpaired *t*-test. Full color version is available within the online issue.
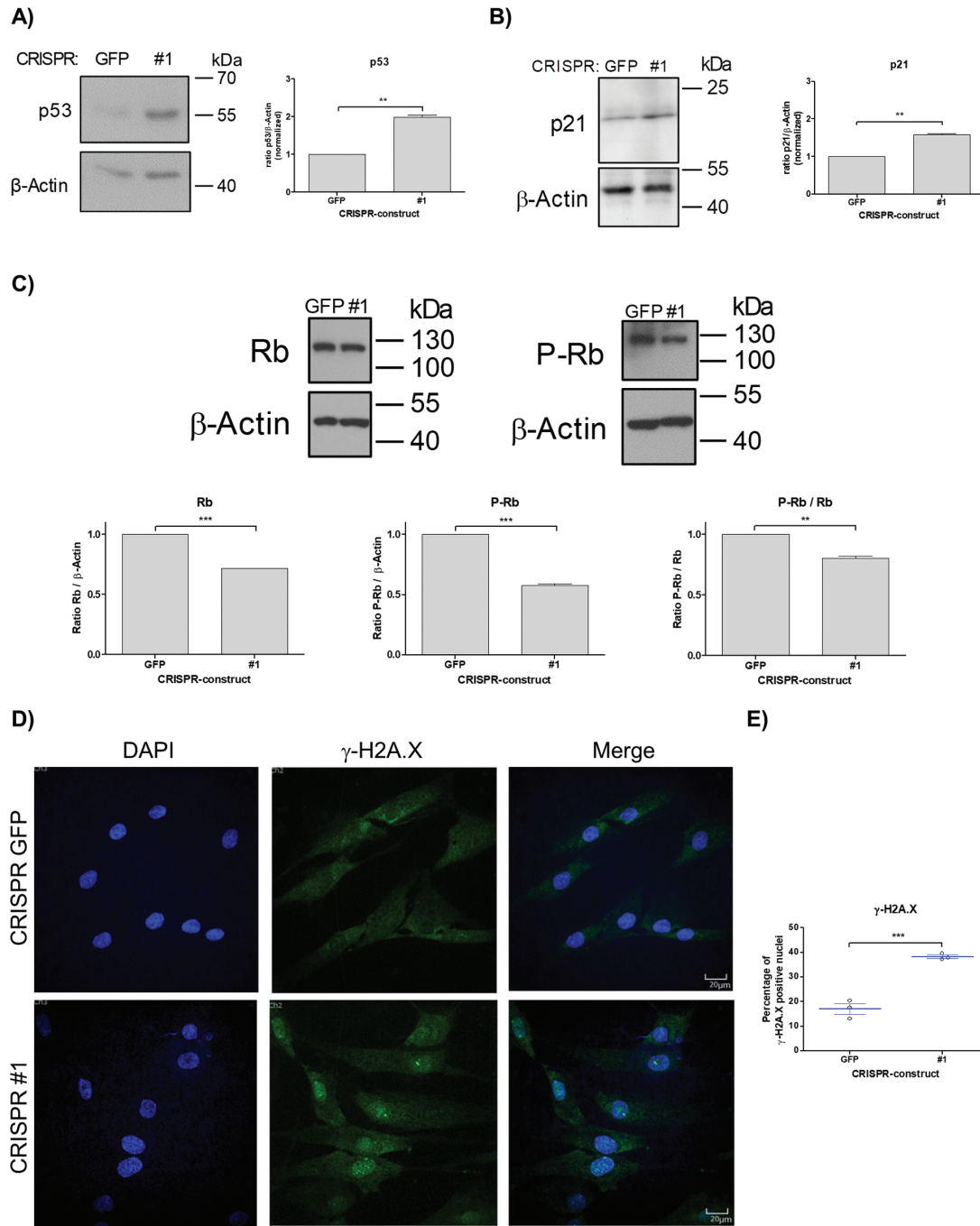
Figure 3. Mechanism of senescence in *SPRY1* KO adipose stem/progenitor cells (ASCs). (**A**) Western blot analysis of p53 protein level. Left panel: A representative Western blot result of $n = 3$ independent experiments (ASCs from three different donors) is shown. β-Actin served as loading control. Molecular masses are given in kDa. Right panel: Densitometric quantification. Values are normalized to appropriate CRISPR-GFP control cells and presented as mean ± SEM of three measurements. Statistical comparison was achieved using the Paired two-tailed *t*-test. (**B**) Western blot analysis of p21 protein level. Left panel: A representative Western blot result of $n = 3$ independent experiments (ASCs from three different donors) is shown. Molecular masses are given in kDa. β-Actin served as loading control. Right panel: Densitometric quantification. Values are normalized to appropriate CRISPR-GFP control cells and presented as mean ± SEM of three measurements. Statistical comparison was achieved using the Paired two-tailed *t*-test. (**C**) Western blot analysis of Rb and Phospho(P)-Rb protein level. Upper panel: A representative result of $n = 3$ independent experiments (ie, donors) is shown. Lower panel: Densitometric quantification and calculation of (P)-Rb/Rb ratio. Values are normalized to appropriate CRISPR-GFP control cells and presented as mean ± SEM of three measurements. Statistical comparison was achieved using the Paired two-tailed *t*-test. (**D**) γ-H2A.X staining and analysis of senescence associated heterochromatin foci (SAHF). Representative microphotographs of transduced ASCs from $n = 3$ independent experiments (ie, donors) are shown. Immunofluorescence staining was carried out using a specific antibody against γ-H2A.X (middle panel). Nuclear DNA was stained by DAPI (left panel). Magnification 400×. Scale bar: 20 μm. (**E**) Quantification of γ-H2A.X-positive nuclei in ASCs from three independent donors. At least 500 cells per donor were counted. Values are presented as mean ± SEM of $n = 3$ different donors. Statistical comparison between group was done using the unpaired two-tailed *t*-test. Full color version is available within the online issue.
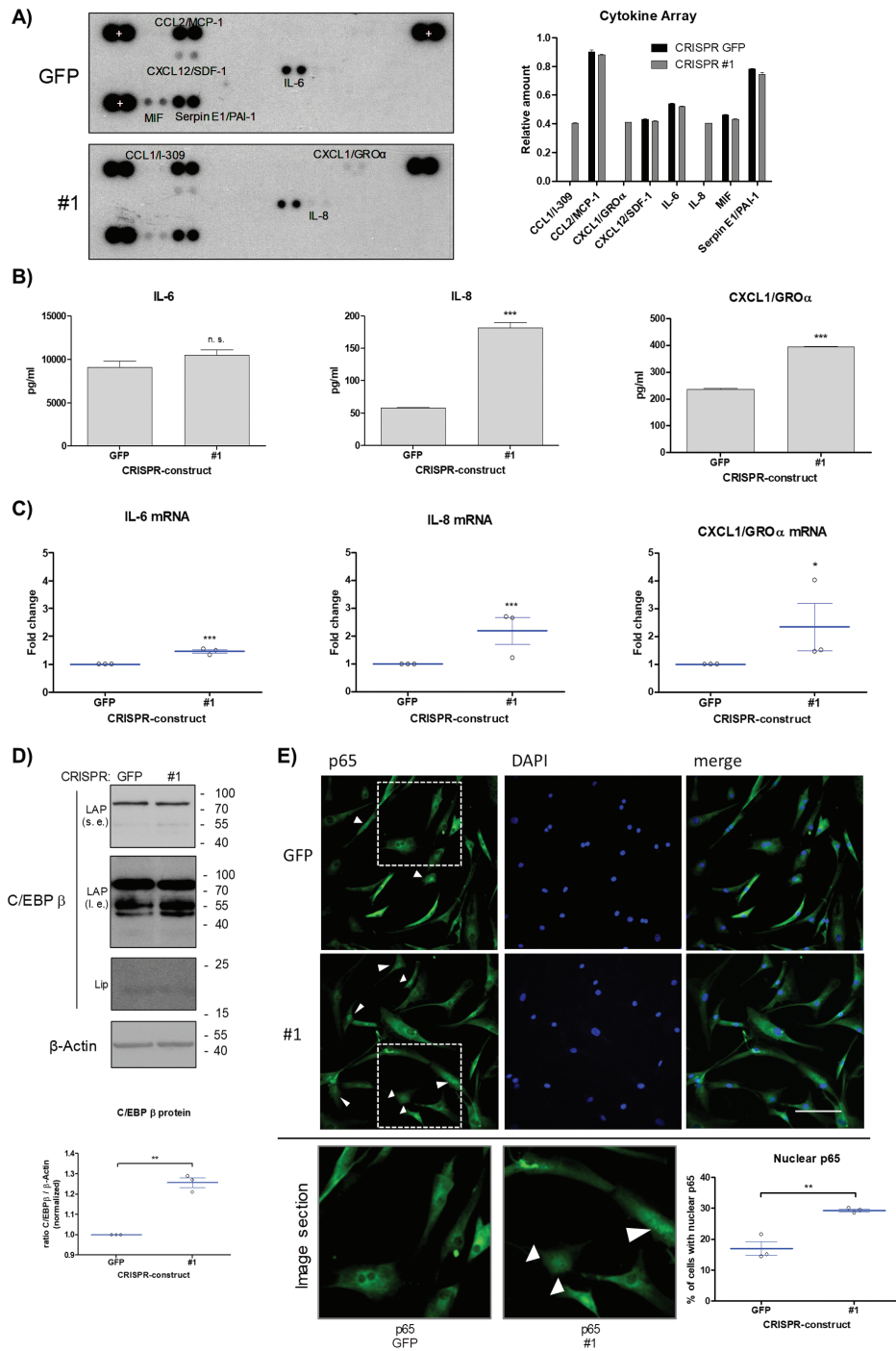
Figure 4. Analysis of CRISPR/Cas9-mediated *SPRY1* KO induced senescence-associated secretory phenotype (SASP) in human ASCs. (**A**) Human Cytokine Array (Proteome Profiler, RnD Systems, #ARY005B). Left panel: adipose stem/progenitor cells (ASCs) were seeded in six-well plates at a density of 5×10^4 cells/well followed by an incubation of 72 hours using PM4 medium (1 mL/well). Corresponding cell culture supernatants of ASCs derived from *n* = 3 different donors were equally pooled and subjected to cytokine profiling. An X-ray film showing two developed cytokine arrays is presented (inverted picture; exposure time 1 hour). The plus (+) indicates the positive controls for assay development. Right panel: Densitometric quantification of cytokines. Values were normalized to the appropriate positive controls of each array and represent two measurements (each capture antibody was spotted twice). (**B**) ELISA measurements of cell culture supernatants as indicated. Representative result of *n* = 3 independent donors. Values are presented as mean ± SEM of three replicates. Statistical comparison was done using the two-tailed unpaired *t*-test. (**C**) IL-6, IL-8, and CXCL1/GROα mRNA expression of *n* = 3 different donors. Values are given as mean ± SEM. Statistical analysis was done using the Paired two-tailed *t*-test. (**D**) Western blot analysis of C/EBPβ. Upper panel: A representative Western blot experiment in lysates of ASCs out of *n* = 3 independent donors is shown. Molecular masses are given in kDa. β-Actin served as loading control. Bottom panel: Densitometric quantification of C/EBPβ protein levels in ASCs derived from *n* = 3 different donors. Statistical comparison was done using the Paired two-tailed *t*-test. (**E**) Subcellular localization of the NF-κB subunit p65 in human ASCs. Cells were processed for indirect immunofluorescence microscopy and viewed using a confocal scanning system. Cells were stained with anti-p65 antibodies (left panel) as indicated. DAPI (middle panel) served as nuclear stain. A representative result of *n* = 3 different experiments (ie, donors) is shown. Arrow heads indicate nuclear staining of p65. Scale bar: 150 μm. Selected image sections are magnified for clarity. Inlet: Quantification of nuclear p65. Values are presented as mean ± SEM of *n* = 3 donors. Statistical comparison was done using the two-tailed unpaired *t*-test. Full color version is available within the online issue.
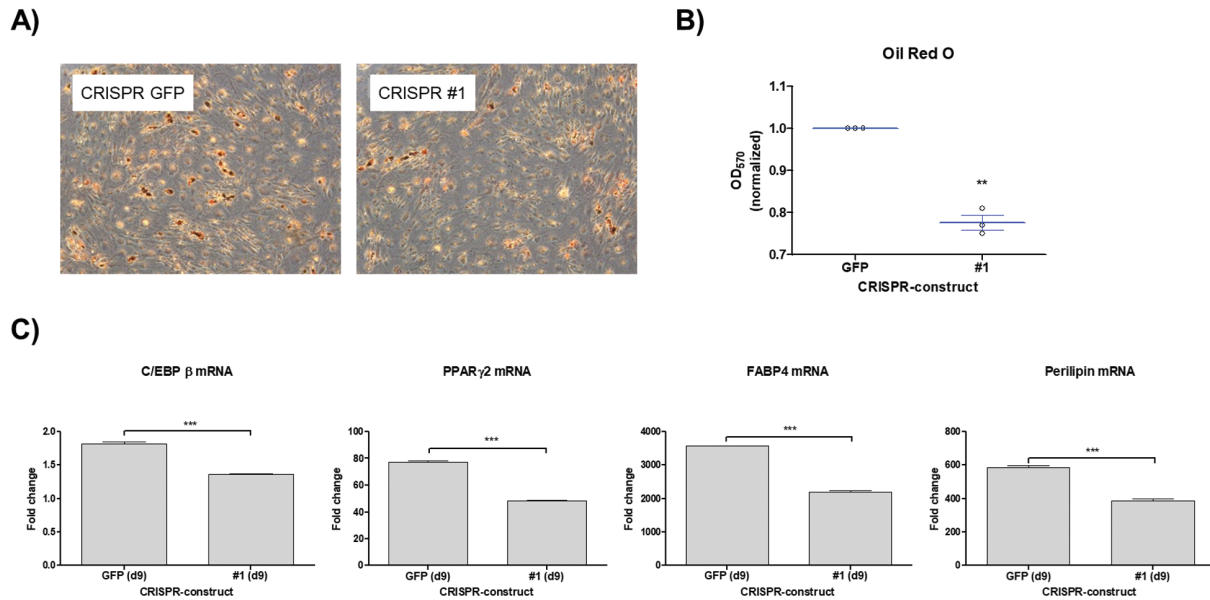
Figure 5. Adipogenic differentiation of *SPRY1* KO ASCs. (**A**) Oil Red O staining of differentiated CRISPR/Cas9 expressing adipose stem/progenitor cells (ASCs) is shown as indicated. Cells were stained on Day 14 postinduction of adipogenesis. Magnification 50×. (**B**) Photometric quantification of Oil Red O staining of ASCs from $n = 3$ different donors. Values are presented as mean ± SEM. Statistical comparison was achieved using one-way ANOVA and Dunnett's Multiple Comparison Test. (**C**) Expression of adipogenic signature genes as indicated on Day 9 of adipogenic differentiation (normalized to undifferentiated control cells [Day 0]). Statistical comparison was done with the two-tailed Unpaired *t*-test. A representative result of $n = 3$ independent experiments (ie, donors) is shown. Full color version is available within the online issue.

Adipogenesis Is Impaired in Senescent Human SPRY1 KO ASCs

Recently, we showed that Sprouty1 depletion by RNA interference inhibited adipogenic differentiation of ASCs (23). Since senescence prevents differentiation in ASCs (10) and other cell types (14), we hypothesized that Sprouty1 KO induced senescence leads to impaired adipogenesis in ASCs. To test this, CRISPR-construct #1 ASCs and control cells were subjected to adipogenic differentiation. Afterwards, intracellular lipid accumulation was assayed by Oil Red O staining on Day 14 postinduction of differentiation. *SPRY1* KO cells accumulated considerably less lipids compared to CRISPR-GFP control ASCs (Figure 5A and B). Moreover, the expression of adipogenic marker genes was significantly inhibited in *SPRY1* KO cells (Figure 5C). These results demonstrate that *SPRY1* KO in ASCs leads to senescence, and hence, impaired adipogenesis. Thus, the expression of SPRY1 needs to be tightly controlled in ASCs to maintain proliferation and adipogenic differentiation potential.

Discussion

ASCs contribute to adipose tissue homeostasis, regeneration, and expansion (41). However, the capacity of ASCs to divide and differentiate declines during adulthood and is very low in the older adults (7,9–13,22,42,43). Similarly, the contribution of ASC hyperplasia to expansion of adipose tissue in adulthood obesity is rather low (41,44,45). In accordance with these findings, evidence from several studies indicates that the accumulation of senescent cells in adipose tissues is a hallmark of aging and obesity causing functional decline (7,9–12,22). WL interventions prevent obesity and extend healthy life span of formerly obese people (2,3). The impact of WL on ASCs is little understood. We have shown that this intervention holds adipogenesis at a low rate, protects against DNA damage, improves

survival, and postpones replicative senescence of ASCs derived from formerly obese people (22). This suggests that WL protects ASCs and improves their functionality for a longer period. Analyzing the underlying mechanisms, we found that WL induces DIRAS3 leading to reduced PI3K/Akt/mTOR signaling and prevention of premature senescence in ASCs of formerly obese people (9,24). Recently, we demonstrated that WL induces the expression of Sprouty1 a negative regulator of Ras-MAPK signaling. Silencing of Sprouty1 in ASCs hyper-activated MAPK signaling and impaired adipogenesis (23). However, reducing ERK phosphorylation by a MEK inhibitor could not rescue adipogenic differentiation in Sprouty1 KD ASCs (23). Thus, the mechanism by which Sprouty1 regulates adipogenesis in ASCs remained incompletely understood. In our present study, we show that the inhibition of Sprouty1 expression in ASCs induces a senescence-like phenotype blocking proliferation and adipogenesis. This suggests that Sprouty1, by preventing over-activation of mitogenic signaling, avoids senescence in human ASCs and thereby maintains the proliferative and adipogenic differentiation capacity of this adult stem/progenitor cell type. Together with previous studies from our group on the protective effect of WL against ASC senescence (10,22) and on the role of DIRAS3 (9,24) and Sprouty1 (23) in this scenario, our present study indicates that WL-induced deceleration of signaling through the two main downstream signaling cascades of the Insulin/IGF-1 pathway protects ASCs against premature senescence and is important for adipose tissue homeostasis and expansion.

Senescent cells are defined by several hallmarks, such as a permanent growth arrest and expression of senescence marker (14,46); however, there is still a lack of a single specific marker for cellular senescence and even p16[Ink4A] is expressed in certain nonsenescent cells and is not expressed by all senescent cells (46). Moreover, different senescence programs exist and the cellular senescence phenotype is highly variable (46). As shown in our present study, Sprouty1 depletion in

ASCs caused an antiproliferative effect accompanied with cell enlargement and SA β-Gal positivity, which represent common features of senescent cells ([14]). Cellular senescence requires activation of Rb either by activation of p16[INK4A], the p53/p21[Cip1] pathway, or both ([14]). We show that the depletion of Sprouty1 in ASCs strongly activates the p53/p21[Cip1] pathway. These data are in accordance with the seminal study by Minamino and colleagues ([7]), which demonstrated a crucial role of the p53/p21[Cip1] pathway for the induction of stress-induced senescence in adipose tissues of obese and diabetic mice and humans. A p16[INK4A] response was barely detectable neither on mRNA nor protein level in the senescent Sprouty1 KO ASCs in our study (data not shown). Thus, according to the current models ([47]), the loss of the function of Sprouty1 might induce an early senescence phenotype in human ASCs in which the p16[INK4A] protein is absent and/or not yet expressed. It is well known that p21[Cip1] blocks cyclin-dependent kinases (ie, CDK2 and CDK4/6), which phosphorylate Rb, p107, and p130 to facilitate cell-cycle progression ([48,49]). The particular contribution of these pocket proteins to cellular senescence is not completely understood and among others cell-type dependent ([49,50]). In our present study, we observed a consistent activation (hypo-phosphorylation) of Rb in *SPRY1* KO ASCs. In addition, Rb protein levels were reduced in *SPRY1* KO ASCs compared to control cells. These findings are in agreement with the previous observations and the concept that Rb is dispensable at later stages of senescence ([51]). We also analyzed the two other members of the Rb family proteins p107 and p130 showed no clear pattern up to 20 days after the *SPRY1* KO (data not shown).

By applying the CRISPR/Cas9 approach, we recognized a considerable induction of γ-H2A.X-positive SAHFs in *SPRY1* KO ASCs relative to CRISPR-GFP control ASCs, which is indicative for an activated DNA-damage response (DDR) in the Sprouty1-depleted cells. Given the fact that not all senescence programs are a consequence of a DDR ([14]), this finding suggests that Sprouty1 loss-of-function induced senescence in ASCs is likely linked to DDR-induced senescence, which also comprises oncogene-induced senescence, for example, following overexpression of oncogenic Ras ([52]) or constitutive activation of MAPK ([35]). In contrast to the Sprouty1 KO overexpression of oncogenic Ras in human fibroblasts has been shown to induce both a strong p21[Cip1] and p16[Ink4A] response, suggesting that the pro-senescence signal elicited by loss of function of Sprouty1 (one out of several specific negative regulators of Ras-MAPK signaling) is milder.

Senescent cells are known to secrete a specific pattern of proinflammatory factors including cytokines and growth factors and extra cellular matrix modulating proteins, known as the SASP, which attributes autocrine, paracrine, and endocrine activities to senescent cells with beneficial and deleterious effects ([17]). The SASP is, for example, beneficial in wound healing processes and promote the clearing of senescent cells by the immune system. However, the accumulation of senescent cells in obesity ([7]) and aging ([12]) is predominantly associated with detrimental effects. Among the proinflammatory factors, IL-6, IL-8, CXCL1/GROα, and some others are specific signature cytokines of the SASP ([53]). It has been found that the SASP can be highly variable. In fact, it can differ between given cellular senescence phenotypes ([17]). By employing a cytokine array that can detect 36 different cytokines, we identified a specific secretory phenotype of *SPRY1* KO ASCs. Associated with the activation of the two major SASP-inducing transcription factors, C/EBP β and NF-κB, these cells induced the secretion of CXCL1/GROα and IL-8 compared to CRISPR-GFP control ASCs. We have previously shown that the secretion of IL-8 is also specifically upregulated in

DIRAS3 KD-induced cellular senescence of human ASCs ([9]). Roldan and colleagues (2011) ([54]) demonstrated upregulation of IL-8 in senescent ASCs isolated from omental adipose biopsies of obese humans. These studies underscore a role of IL-8 in obesity-related senescence. The secretion of CXCL1/GROα was previously associated with the SASP of senescent fibroblasts ([53]) and demonstrated to act in an autocrine and paracrine manner probably to modulate proliferation and differentiation ([14]). Moreover, Zhang and colleagues ([55]) showed that CXCL1/GROα functions as a chemoattractant in obesity-associated ASC trafficking. This effect was further confirmed in a murine model and shown to be dependent on CXCR1 receptor signaling ([55]). Thus, increasing evidence suggests that CXCL1/GROα plays an important role in the obesity-associated SASP.

The role of Sprouty1 in adipose tissue in vivo was extensively studied by Urs and colleagues ([29,56]). Employing a murine model with ap2 promotor-dependent expression or deletion of *spry1* in adipose tissue, the authors demonstrated that Sprouty1 over-expression confers a protective effect against high-fat diet-induced fat accumulation ([56]). Sprouty1 loss-of-function was associated with high body fat ([29]). These studies underscore the importance of Sprouty1 in adipose tissue. In our studies, which specifically address Sprouty1 depletion in ASCs, we demonstrate that Sprouty1 depletion prevents adipogenic differentiation by a cellular senescence-dependent mechanism resembling the obesity and diabetes-related p53/p21[Cip1] senescence phenotype in adipose tissues shown by Minamino and colleagues ([7]). Overexpression of Sprouty1 has no significant effects on adipogenesis and/or proliferation in these human adipose stem/progenitor cells.

In conclusion, our study suggests a novel mechanism by which Sprouty1 affects the fate of human ASCs after WL. Upregulation of Sprouty1 by WL protects ASCs against senescence and supports proper self-renewal and adipogenesis capacity. Lower levels of Sprouty1 in ASCs of adipose tissues of obese people might increase the likelihood of acquiring a senescence phenotype concomitant with impaired proliferation and adipogenic differentiation and the development of senescence-associated inflammation.

Supplementary Material

Supplementary data are available at *The Journals of Gerontology, Series A: Biological Sciences and Medical Sciences* online.

Supplementary Table 1. Clinical data. Human sWAT samples were obtained from the lower abdomen of healthy donors undergoing routine abdominoplasty at the Institute for Plastic and Reconstructive Surgery at the Medical University of Innsbruck, Austria. WL interventions prior surgery are indicated. BMI: Body mass index; NWD: Normal weight donor; WLD: weight loss donor, which was formerly obese, f = female, m = male, n. a. = not available.

Supplementary Table 2. Sequences of DNA oligos required for CRISPR/Cas9-vector cloning. CRISPR/Cas9 target sequences corresponding to the human *SPRY1* gene or the non-human *gfp* gene are highlighted.

Supplementary Table 3. Antibodies for Western blotting.

Supplementary Table 4. Primer sequences for RT-qPCR analysis in human cells

Supplementary Figure S1: Determination of apoptosis in CRISPR/Cas9 expressing ASCs by AnnexinV/PI staining and FACS analysis. Values are presented as mean +/- SEM of *n* = 3 different donors. Statistical analysis was achieved using Two-way ANOVA with Bonferroni post-tests.

Supplementary Figure S2: Cytokine Array as shown in Figure 5 with the appropriate grid-overlay. Coordinates and cytokines are indicated.

Funding

Author Contributions

Ma.M., S.A.W., H.R., A.E., S.B., and W.Z. designed the experiments. Ma.M., S.A.W., F.M.H., H.R., A.E., P.W., H.P.V., and J.S. performed the experiments. Ma.M. and W.Z. wrote the manuscript. W.Z. conceived the study. M.M., M.E.Z., and G.P. provided the adipose tissue samples. All authors read and approved the final version of the manuscript.

Conflict of Interest

None reported.

References

1. Ng M, Fleming T, Robinson M, et al. Global, regional, and national prevalence of overweight and obesity in children and adults during 1980–2013: a systematic analysis for the Global Burden of Disease Study 2013. *Lancet*. 2014;384(9945):766–81. doi: 10.1016/S0140-6736(14)60460–8

2. Everitt AV, Hilmer SN, Brand-Miller JC, et al. Dietary approaches that delay age-related diseases. *Clin Interv Aging*. 2006;1:11–31. doi: 10.2147/ciia.2006.1.1.11

3. Redman LM, Ravussin E. Caloric restriction in humans: impact on physiological, psychological, and behavioral outcomes. *Antioxid Redox Signal*. 2011;14:275–287. doi: 10.1089/ars.2010.3253

4. Louwen F, Ritter A, Kreis NN, Yuan J. Insight into the development of obesity: functional alterations of adipose-derived mesenchymal stem cells. *Obes Rev*. 2018;19:888–904. doi: 10.1111/obr.12679

5. MacLean PS, Higgins JA, Giles ED, Sherk VD, Jackman MR. The role for adipose tissue in weight regain after weight loss. *Obesity Rev*. 2015;16 Suppl 1:45–54. doi: 10.1111/obr.12255

6. Burton DGA, Faragher RGA. Obesity and type-2 diabetes as inducers of premature cellular senescence and ageing. *Biogerontology*. 2018;19:447–459. doi: 10.1007/s10522-018-9763-7

7. Minamino T, Orimo M, Shimizu I, et al. A crucial role for adipose tissue p53 in the regulation of insulin resistance. *Nat Med*. 2009;15:1082–1087. doi: 10.1038/nm.2014

8. Salvestrini V, Sell C, Lorenzini A. Obesity may accelerate the aging process. *Front Endocrinol (Lausanne)*. 2019;10:266. doi: 10.3389/fendo.2019.00266

9. Ejaz A, Mattesich M, Zwerschke W. Silencing of the small GTPase DIRAS3 induces cellular senescence in human white adipose stromal/progenitor cells. *Aging (Albany NY)*. 2017;9:860–879. doi: 10.18632/aging.101197

10. Mitterberger MC, Lechner S, Mattesich M, Zwerschke W. Adipogenic differentiation is impaired in replicative senescent human subcutaneous adipose-derived stromal/progenitor cells. *J Gerontol A Biol Sci Med Sci*. 2014;69:13–24. doi: 10.1093/gerona/glt043

11. Xu M, Palmer AK, Ding H, et al. Targeting senescent cells enhances adipogenesis and metabolic function in old age. *Elife*. 2015;4:e12997. doi: 10.7554/eLife.12997

12. Baker DJ, Childs BG, Durik M, et al. Naturally occurring p16(Ink4a)-positive cells shorten healthy lifespan. *Nature*. 2016;530:184–189. doi: 10.1038/nature16932

13. Guillermier C, Fazeli PK, Kim S, et al. Imaging mass spectrometry demonstrates age-related decline in human adipose plasticity. *JCI Insight*. 2017;2:e90349. doi: 10.1172/jci.insight.90349

14. van Deursen JM. The role of senescent cells in ageing. *Nature*. 2014;509:439–446. doi: 10.1038/nature13193

15. Salotti J, Johnson PF. Regulation of senescence and the SASP by the transcription factor C/EBPβ. *Exp Gerontol*. 2019;128:110752. doi: 10.1016/j.exger.2019.110752

16. Da Silva-Álvarez S, Picallos-Rabina P, Antelo-Iglesias L, et al. The development of cell senescence. *Exp Gerontol*. 2019;128:110742. doi: 10.1016/j.exger.2019.110742

17. Malaquin N, Martinez A, Rodier F. Keeping the senescence secretome under control: Molecular reins on the senescence-associated secretory phenotype. *Exp Gerontol*. 2016;82:39–49. doi: 10.1016/j.exger.2016.05.010

18. Smith DL Jr, Yang Y, Nagy TR, et al. Weight cycling increases longevity compared with sustained obesity in mice. *Obesity (Silver Spring)*. 2018;26:1733–1739. doi: 10.1002/oby.22290

19. Bodkin NL, Alexander TM, Ortmeyer HK, Johnson E, Hansen BC. Mortality and morbidity in laboratory-maintained Rhesus monkeys and effects of long-term dietary restriction. *J Gerontol A Biol Sci Med Sci*. 2003;58:212–219. doi: 10.1093/gerona/58.3.b212

20. Rueda-Clausen CF, Ogunleye AA, Sharma AM. Health benefits of long-term weight-loss maintenance. *Annu Rev Nutr*. 2015;35:475–516. doi: 10.1146/annurev-nutr-071714-034434

21. Mitterberger MC, Mattesich M, Klaver E, et al. Adipokine profile and insulin sensitivity in formerly obese women subjected to bariatric surgery or diet-induced long-term caloric restriction. *J Gerontol A Biol Sci Med Sci*. 2010;65:915–923. doi: 10.1093/gerona/glq107

22. Mitterberger MC, Mattesich M, Zwerschke W. Bariatric surgery and diet-induced long-term caloric restriction protect subcutaneous adipose-derived stromal/progenitor cells and prolong their life span in formerly obese humans. *Exp Gerontol*. 2014;56:106–113. doi: 10.1016/j.exger.2014.03.030

23. Mandl M, Wagner SA, Hatzmann FM, et al. Sprouty1 is a weight-loss target gene in human adipose stem/progenitor cells that is mandatory for the initiation of adipogenesis. *Cell Death Dis*. 2019;10:411. doi: 10.1038/s41419-019-1657-3

24. Ejaz A, Mitterberger MC, Lu Z, et al. Weight loss upregulates the small GTPase DIRAS3 in human white adipose progenitor cells, which negatively regulates adipogenesis and activates autophagy via Akt-mTOR inhibition. *EBioMedicine*. 2016;6:149–161. doi: 10.1016/j.ebiom.2016.03.030

25. Cabrita MA, Christofori G. Sprouty proteins, masterminds of receptor tyrosine kinase signaling. *Angiogenesis*. 2008;11:53–62. doi: 10.1007/s10456-008-9089-1

26. Lake D, Corrêa SA, Müller J. Negative feedback regulation of the ERK1/2 MAPK pathway. *Cell Mol Life Sci*. 2016;73:4397–4413. doi: 10.1007/s00018-016-2297-8

27. Kim HJ, Bar-Sagi D. Modulation of signalling by Sprouty: a developing story. *Nat Rev Mol Cell Biol*. 2004;5:441–450. doi: 10.1038/nrm1400

28. Masoumi-Moghaddam S, Amini A, Morris DL. The developing story of Sprouty and cancer. *Cancer Metastasis Rev*. 2014;33:695–720. doi: 10.1007/s10555-014-9497-1

29. Urs S, Venkatesh D, Tang Y, et al. Sprouty1 is a critical regulatory switch of mesenchymal stem cell lineage allocation. *FASEB J*. 2010;24:3264–3273. doi: 10.1096/fj.10-155127

30. Chakkalakal JV, Jones KM, Basson MA, Brack AS. The aged niche disrupts muscle stem cell quiescence. *Nature*. 2012;490:355–360. doi: 10.1038/nature11438

31. Shea KL, Xiang W, LaPorta VS, et al. Sprouty1 regulates reversible quiescence of a self-renewing adult muscle stem cell pool during regeneration. *Cell Stem Cell*. 2010;6:117–129. doi: 10.1016/j.stem.2009.12.015

32. Abou-Khalil R, Brack AS. Muscle stem cells and reversible quiescence: the role of sprouty. *Cell Cycle*. 2010;9:2575–2580. doi: 10.4161/cc.9.13.12149

33. Liu W, Klose A, Forman S, et al. Loss of adult skeletal muscle stem cells drives age-related neuromuscular junction degeneration. *eLife*. 2017;6. doi: 10.7554/eLife.26464

34. Slack C. Ras signaling in aging and metabolic regulation. *Nutr Healthy Aging*. 2017;4:195–205. doi: 10.3233/NHA-160021

35. Lin AW, Barradas M, Stone JC, van Aelst L, Serrano M, Lowe SW. Premature senescence involving p53 and p16 is activated in response to constitutive MEK/MAPK mitogenic signaling. *Genes Dev*. 1998;12:3008–3019. doi: 10.1101/gad.12.19.3008

36. Sanjana NE, Shalem O, Zhang F. Improved vectors and genome-wide libraries for CRISPR screening. *Nat Methods*. 2014;11:783–784. doi: 10.1038/nmeth.3047

37. Shalem O, Sanjana NE, Hartenian E, et al. Genome-scale CRISPR-Cas9 knockout screening in human cells. *Science*. 2014;343:84–87. doi: 10.1126/science.1247005

38. Huo W, Zhao G, Yin J, et al. Lentiviral CRISPR/Cas9 vector mediated miR-21 gene editing inhibits the epithelial to mesenchymal transition in ovarian cancer cells. *J Cancer*. 2017;8:57–64. doi: 10.7150/jca.16723

39. Yin Y, Zhong J, Li SW, et al. TRIM11, a direct target of miR-24-3p, promotes cell proliferation and inhibits apoptosis in colon cancer. *Oncotarget*. 2016;7:86755–86765. doi: 10.18632/oncotarget.13550

40. Mitterberger MC, Lechner S, Mattesich M, et al. DLK1(PREF1) is a negative regulator of adipogenesis in CD105+/CD90+/CD34+/CD31–/FABP4– adipose-derived stromal cells from subcutaneous abdominal fat pats of adult women. *Stem Cell Res*. 2012;9:35–48. doi: 10.1016/j.scr.2012.04.001

41. Spalding KL, Arner E, Westermark PO, et al. Dynamics of fat cell turnover in humans. *Nature*. 2008;453:783–787. doi: 10.1038/nature06902

42. Borkan GA, Hults DE, Gerzof SG, Robbins AH, Silbert CK. Age changes in body composition revealed by computed tomography. *J Gerontol*. 1983;38:673–677. doi: 10.1093/geronj/38.6.673

43. Kirkland JL, Tchkonia T, Pirtskhalava T, Han J, Karagiannides I. Adipogenesis and aging: does aging make fat go MAD? *Exp Gerontol*. 2002;37:757–767. doi: 10.1016/s0531-5565(02)00014-1

44. Kim SM, Lun M, Wang M, et al. Loss of white adipose hyperplastic potential is associated with enhanced susceptibility to insulin resistance. *Cell Metab*. 2014;20:1049–1058. doi: 10.1016/j.cmet.2014.10.010

45. Wang QA, Tao C, Gupta RK, Scherer PE. Tracking adipogenesis during white adipose tissue development, expansion and regeneration. *Nat Med*. 2013;19:1338–1344. doi: 10.1038/nm.3324

46. Gorgoulis V, Adams PD, Alimonti A, et al. Cellular senescence: defining a path forward. *Cell*. 2019;179:813–827. doi: 10.1016/j.cell.2019.10.005

47. Mijit M, Caracciolo V, Melillo A, Amicarelli F, Giordano A. Role of p53 in the Regulation of Cellular Senescence. *Biomolecules*. 2020;10(3). doi: 10.3390/biom10030420

48. Uxa S, Bernhart SH, Mages CFS, et al. DREAM and RB cooperate to induce gene repression and cell-cycle arrest in response to p53 activation. *Nucleic Acids Res*. 2019;47:9087–9103. doi: 10.1093/nar/gkz635

49. Cobrinik D. Pocket proteins and cell cycle control. *Oncogene*. 2005;24:2796–2809. doi: 10.1038/sj.onc.1208619

50. Alessio N, Capasso S, Ferone A, et al. Misidentified human gene functions with mouse models: the case of the retinoblastoma gene family in senescence. *Neoplasia*. 2017;19:781–790. doi: 10.1016/j.neo.2017.06.005

51. Helmbold H, Galderisi U, Bohn W. The switch from pRb/p105 to Rb2/p130 in DNA damage and cellular senescence. *J Cell Physiol*. 2012;227:508–513. doi: 10.1002/jcp.22786

52. Serrano M, Lin AW, McCurrach ME, Beach D, Lowe SW. Oncogenic ras provokes premature cell senescence associated with accumulation of p53 and p16INK4a. *Cell*. 1997;88:593–602. doi: 10.1016/s0092-8674(00)81902-9

53. Rodier F, Campisi J. Four faces of cellular senescence. *J Cell Biol*. 2011;192:547–556. doi: 10.1083/jcb.201009094

54. Roldan M, Macias-Gonzalez M, Garcia R, Tinahones FJ, Martin M. Obesity short-circuits stemness gene network in human adipose multipotent stem cells. *FASEB J*. 2011;25:4111–4126. doi: 10.1096/fj.10-171439

55. Zhang T, Tseng C, Zhang Y, et al. CXCL1 mediates obesity-associated adipose stromal cell trafficking and function in the tumour microenvironment. *Nat Commun*. 2016;7:11674. DOI: 10.1038/ncomms11674

56. Urs S, Henderson T, Le P, Rosen CJ, Liaw L. Tissue-specific expression of Sprouty1 in mice protects against high-fat diet-induced fat accumulation, bone loss and metabolic dysfunction. *Br J Nutr*. 2012;108:1025–1033. doi: 10.1017/S0007114511006209